Understanding traffic jams using quantum algorithms

Tomi H. Johnson

(Dated: April 30, 2009)

An algorithm developed for studying the time evolution of weakly entangled one-dimensional (1D) quantum systems is extended to simulate stochastic classical systems. The accuracy and applicability of the algorithm are examined using a number of classical 1D lattice models, which are interpreted in terms of vehicular traffic. Notably, the algorithm is successfully used to describe time evolution away from steady-state. Such situations are difficult to simulate using current methods. Thus the algorithm opens up new possibilities for studying the dynamical behaviour of stochastic classical systems.

I. INTRODUCTION

Traffic jams are a problem that many of us face daily. A 2007 report estimated that the average American spends 38 hours a year in traffic, costing $78 billion[1]. Such impacts have created a demand to understand and, if possible, control vehicular traffic and its phenomena. Scientific interest in traffic has grown considerably over the last two decades, partly for the above reason and partly due to the development of large-scale computer simulations[2].

Early scientific approaches to traffic concentrated on macroscopic methods. One such method was to model traffic as a fluid, constructing Navier-Stokes-like equations to describe its flow[3]. Another method treated traffic like a gas of interacting particles, describing it by modifying the kinetic theory of gasses[4]. Recently the focus has been on microscopic approaches, of which particular attention has been paid to the NaSch model and its extensions[5]. In these, vehicles are described as particles moving on a lattice, with time, speed and acceleration discretised. The location, speed and acceleration of each particle is updated at each time-step according to a set of probabilistic rules. These systems are studied using Monte Carlo methods, which obtain statistical properties by averaging over a large number of simulations. Models of this type have been successful in reproducing steady-state features of real traffic systems, such as phase changes and self-organised criticality (see [6, 7] for reviews).

Another approach, which I took in this project, is to apply models from stochastic non-equilibrium physics. These so-called particle hopping systems have the following features: particles occupy a 1D lattice; the boundary sites are connected to particle reservoirs, so particles are injected and ejected there; and a hopping process causes particles to move through the lattice (see [8, 9] for a review). The quintessential example is the totally asymmetric exclusion process (TASEP)[10–13], shown in Fig. 1. Like the Ising and Heisenberg models of equilibrium statistical physics[14], simple particle hopping systems are archetypal of non-equilibrium physics. Unlike equilibrium statistical mechanics, there is no complete framework to understand non-equilibrium behaviour, especially away from steady-state, which motivates its study. Particle hopping systems also have applications to vehicular traffic flow[6, 7, 15], biological transport[16–19] and other driven diffusive processes[8].

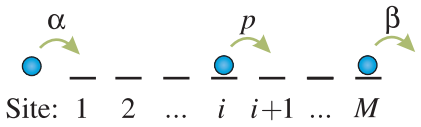

FIG. 1: The TASEP is a typical stochastic non-equilibrium system. Particles are injected into the 1st site with rate α if it is empty and ejected from the M-th site with rate β if occupied. Particles in the i-th site hop to the $(i+1)$-th site with a rate p if that site is empty, resulting in flow from left to right.

A combination of analytical results[8] and Monte Carlo simulations[6, 16, 20] have been used to investigated these systems. Exact steady-state solutions for many simple models have been found, including the TASEP[21]. The steady-states may also be calculated numerically using the density matrix renormalisation group (DMRG) method[22, 23] (see [24] for a recent review). In 1998 Hieida used the DMRG to determine the steady-state of the TASEP[25]. Excellent agreement with the exact analytical solution was found. Since then, others have applied the DMRG method to more complicated systems with similar success[26, 27].

However, these methods can only be used to study steady-states. For a complete understanding of these models and the phenomena they hope to describe, a method is required to investigate the time evolution away from steady-state. There have been few successes in simulating time evolution using Monte Carlo techniques; it took until 2008 for the time evolution of the TASEP to be studied, under restricted conditions[28]. Thus there is a need for a numerical method that can do

this.

In this report I introduce such a numerical method to simulate time evolution, as well as steady-states. I demonstrate that efficient, near-exact simulation of stochastic classical systems is possible, by applying it to traffic flow. The method is an adaptation of a numerical scheme, originally proposed in 2003 to classically simulate quantum computations, called the time-evolving block decimation (TEBD) algorithm. It was shown that efficient near-exact simulation is possible for weakly entangled computations[29]. Soon after this, the algorithm was extended to simulate the time evolution of 1D quantum lattice systems, provided entanglement is sufficiently restricted[30]. A key feature of the TEBD algorithm is that the system's most relevant degrees of freedom are identified and kept, while those less relevant are neglected. This is achieved by representing the quantum state by a product of matrices[31, 32], which are updated according to the evolution of the system. This matrix product representation (MPR) of the states allows the identification and truncation of unimportant degrees of freedom. This prevents the exponential growth of computing resources required to represent the quantum state, and thus allows simulation using a classical computer. A more detailed description of the algorithm will be given in later sections. For a broad class of 1D quantum systems it has been shown that entanglement is sufficiently restricted such that only a small number of degrees of freedom are required to approximate the system well[33–35]. Consequently, a wide range of 1D quantum systems have been successfully simulated by the algorithm, including spin chains[30, 36] and Bose-Hubbard models[37]. To my knowledge the algorithm has not yet been applied to classical systems.

The motivation behind this project is to provide a numerical tool for studying the dynamics of non-equilibrium systems, about which little is currently understood. The eventual goal is to extend the algorithm to investigate a range of classical systems and their phenomena. Accordingly, I focus on how the algorithm works and how it can be adapted to classical systems. Later sections show that this is possible in practice by testing the algorithm with simple traffic models. Sec. II contains an overview of how the TEBD algorithm is able to simulate quantum systems and calculate their properties. In Sec. III, I introduce the class of stochastic classical systems that I will study, highlighting their mathematical similarity to quantum systems. Sec. IV outlines how the TEBD algorithm was adapted for the classical systems, focusing on the differences from the quantum case and difficulties in interpreting the method. In Sec. V, I test the TEBD algorithm's performance by simulating both steady-states and time evolution of traffic models. Sec. VI concludes the report and I propose a range of extensions to the models and algorithm. Details of the models and exact analytical solutions of the TASEP are contained in the appendices.

II. THE TEBD ALGORITHM

A program that implements the TEBD algorithm to simulate the time evolution of quantum systems was provided by S. R. Clark and D. Jaksch. The code is not presented here. Instead I outline, in principle, how the TEBD algorithm works to give an idea of its features and errors. The resources required to classically describe a quantum state exactly increase exponentially with system size, as will be shown presently. Exponential growth of resources is called "inefficient", while growth as a low order polynomial is "efficient". The TEBD algorithm simulates the time evolution of a quantum lattice system efficiently. It does this in three key steps: (i) the state of the system is described approximately; (ii) at each time-step the state is evolved; and (iii) expectation values are calculated. In the next subsections I describe how each of these processes can be done efficiently and to what accuracy.

A. Description of the quantum state

The quantum system to be simulated is composed of M sites in a 1D lattice. Each site has a Hilbert space of dimension d. Hence the state of each site can always be written as a superposition of a set of d basis states $|\tau\rangle$, where $\tau = \{0, 1, ..., d-1\}$. The full Hilbert space of the system is the tensor product[38] of the Hilbert spaces of each site, and thus has dimension d^M. It is spanned by the d^M products of the site basis states $|\boldsymbol{\tau}\rangle = |\tau_1\rangle\,|\tau_2\rangle\,...\,|\tau_M\rangle$, where $\boldsymbol{\tau} = \begin{pmatrix}\tau_1 & \tau_2 & ... & \tau_M\end{pmatrix}$. This means a general state may be written as

$$|\psi\rangle = \sum_{\boldsymbol{\tau}} c_{\boldsymbol{\tau}}\,|\boldsymbol{\tau}\rangle\,, \tag{1}$$

and is described completely by the d^M complex numbers $c_{\boldsymbol{\tau}}$. This number increases exponentially with M and highlights the problem that an exact description of the state is inefficient. As a result, it is only possible to simulate small systems exactly.

Consider a splitting of the 1D lattice into two subsystems, one consisting of sites 1 to k and the other containing sites $k+1$ to M. By performing a Schmidt decomposition (SD)[38] of the state vector Eq. (1), it is always possible to write

$$|\psi\rangle = \sum_{\gamma_k=1}^{\chi_k} \lambda_{\gamma_k}^{[k]} \left|\phi_{\gamma_k}^{[1...k]}\right\rangle \left|\phi_{\gamma_k}^{[k+1...M]}\right\rangle. \tag{2}$$

Similarly to Eq. (1), this is simply the state written as a superposition of product basis states. In this case Eq. (2)

is written in terms of the two subsystems rather than the M sites. The $\lambda_{\gamma_k}^{[k]}$ are called Schmidt coefficients. They are real and non-negative and their squares sum to unity, satisfying normalisation. As a result $\{(\lambda_{\gamma_k}^{[k]})^2\}$ is a probability distribution. The vectors $\left|\phi_{\gamma_k}^{[1\ldots k]}\right\rangle$ and $\left|\phi_{\gamma_k}^{[k+1\ldots M]}\right\rangle$ are called Schmidt vectors and they provide an orthonormal basis for each of the two subsystems respectively. The limit of the sum χ_k is called the Schmidt rank and takes the value of the dimension of the smallest subsystem, i.e. $\chi_k = \min(d^k, d^{M-k})$. The Schmidt coefficients are ordered such that $\lambda_1^{[k]} > \lambda_2^{[k]} > \lambda_3^{[k]}$ etc. and so the degrees of freedom to which they correspond are ordered from most to least important.

The unique measure of the entanglement between the two subsystems, satisfying reasonable requirements[33], is

$$E = -\sum_{\gamma_k=1}^{\chi_k} (\lambda_{\gamma_k}^{[k]})^2 \log_2 (\lambda_{\gamma_k}^{[k]})^2. \tag{3}$$

This is also the Von Neumann entropy of the subsystems and the Shannon entropy of the probability distribution $\{(\lambda_{\gamma_k}^{[k]})^2\}$[38]. The entanglement is maximal when the distribution of Schmidt coefficients is uniform and each degree of freedom is equally important. In this case it is not useful to neglect any of the degrees of freedom. It follows from the normalisation of the Schmidt coefficients and the form of Eq. (3) that if entanglement is weak then some Schmidt coefficients are significantly larger than others. Due to the way they are ordered, this means that $\lambda_{\gamma_k}^{[k]}$ decays quickly with increasing γ_k. In this case the state is well approximated by neglecting the degrees of freedom that are unimportant due to their small Schmidt coefficients. Only the most relevant part of the decomposition is kept by setting

$$|\psi\rangle = \sum_{\gamma_k=1}^{\chi_e} \lambda_{\gamma_k}^{[k]} \left|\phi_{\gamma_k}^{[1\ldots k]}\right\rangle \left|\phi_{\gamma_k}^{[k+1\ldots M]}\right\rangle, \tag{4}$$

where $\chi_e < \chi_k$ is the effective Schmidt rank, representing the extent of the truncation. The error of this approximation (the loss of fidelity[38] in the language of quantum information) is equal to the sum of the neglected Schmidt coefficients[30]. For quantum systems such as spin chains, a value of χ_e in the tens or hundreds usually approximates the state well. Compare this to the maximum value of χ_k, which is $d^{M/2}$. For a modest system size $M = 50$ and dimension $d = 4$ this is about 10^{15}, demonstrating the extent to which truncation decreases the resources needed to describe the state.

By applying successive SDs for each of the $M-1$ splittings with $k = 1, 2, \ldots, M-1$, it is possible to write the state as an MPR. By this it is meant that the coefficients of the state can be written as[29, 39]

$$c_{\boldsymbol{\tau}} = \langle L | \mathbf{A}^{[1]\tau_1} \mathbf{A}^{[2]\tau_2} \ldots \mathbf{A}^{[M]\tau_M} | R \rangle . \tag{5}$$

This has a very useful interpretation. Each site has a matrix $\mathbf{A}^{[i]\tau_i}$ assigned to it, dependent on which physical basis state it is in. The coefficients $c_{\boldsymbol{\tau}}$ are found by multiplying these matrices together and turning this into a complex number by taking the inner product with two boundary vectors $\langle L|$ and $|R\rangle$. The dimensions of the i-th site matrices are $(\chi_{i-1} \times \chi_i)$, revealing the relationship between the SDs and the MPR. The state is exactly described by the entries of the matrices. This description still scales exponentially with system size, as the largest matrices will have dimensions $(d^{M/2} \times d^{M/2})$.

Reducing the resources required to describe the state works in the same way as it does for a single SD, by truncating the unimportant degrees of freedom. Truncating the SDs to a maximum Schmidt rank χ_e is equivalent to limiting the number of rows and columns of the matrices to a maximum of χ_e. The error of this approximation is the weight of the neglected Schmidt coefficients, i.e. the sum of those neglected divided by the total[30], and this can be measured. The dimensions of the matrices no longer scale exponentially with the system size. The maximum number of entries in each matrix is χ_e^2 and so the amount of resources required to describe the Md matrices, and thus the state, is $O\left(Md\chi_e^2\right)$. It follows that the truncated MPR is an efficient and accurate way of approximately describing the state, if entanglement is weak.

B. Time evolution

Time evolution of the state is achieved by operating on it with an evolution operator. An operation on a site i will transform the matrix for that site $\mathbf{A}^{[i]\tau_i}$ away from the optimally truncated MPR Eq. (5). Another SD can be performed to bring the state back to an efficient representation. This can be done with a number of computations $O\left(d^2\chi_e^2\right)$[29, 37]. Similarly, performing a two-site nearest-neighbour operation and bringing the state back to an efficient representation requires $O\left(d^4\chi_e^4\right)$ computations. So applying one-site and two-site nearest-neighbour operations on a system's state can be done efficiently while keeping the description of the state efficient.

The evolution operator required to evolve a quantum system with Hamiltonian H for a time δt is $e^{-iH\delta t}$. Consider the time evolution of the state under a Hamiltonian with one-site terms $h^{[i]}$ and nearest-neighbour two-site terms $h^{[i,i+1]}$,

$$H = \sum_{i=1}^{M} h^{[i]} + \sum_{i=1}^{M-1} h^{[i,i+1]} = \sum_{i=1}^{M} H^{[i]}. \tag{6}$$

It is useful to write

$$F = \sum_{\text{even } i} H^{[i]}, \qquad G = \sum_{\text{odd } i} H^{[i]}, \tag{7}$$

so that the Hamiltonian is decomposed as $H = F + G$. F and G do not commute but the second order Suzuki-Trotter expansion[40] can be used to write the evolution operator as

$$e^{-iH\delta t} = e^{-\frac{1}{2}iF\delta t} e^{-iG\delta t} e^{-\frac{1}{2}iF\delta t} + O\left(\delta t^3\right). \quad (8)$$

The terms in F and G commute, because they do not contain operators that act on the same site. Thus $e^{-\frac{1}{2}iF\delta t} = \prod_{\text{even } i} e^{-\frac{1}{2}iH^{[i]}\delta t}$ and $e^{-iG\delta t} = \prod_{\text{odd } i} e^{-iH^{[i]}\delta t}$. Each $e^{-iH^{[i]}}$ is a one-site or two-site nearest-neighbour operator. So the evolution of $|\psi\rangle$ for a time δt is approximately performed by the repeated application of one-site and two-site nearest-neighbour operators. As stated above, these operations can be performed efficiently while also keeping the description of the state efficient. Consequently, this is also true of its time evolution.

Another property of the Suzuki-Trotter expansion is that it approximates the unitary evolution operator by a product of unitary operators. Unitary operators preserve the norm of a state and so time evolution in the TEBD algorithm conserves the norm, up to truncation effects.

C. Calculation of expectation values

A strength of the TEBD algorithm is the ease with which expectation values may be calculated. The expectation value of a general product operator $\hat{O}^{[1]} \otimes \hat{O}^{[2]} \otimes ... \otimes \hat{O}^{[M]}$ is

$$\begin{aligned} &\langle\psi| \hat{O}^{[1]} \otimes \hat{O}^{[2]} \otimes ... \otimes \hat{O}^{[M]} |\psi\rangle \\ &= \langle L*| \mathbf{O}^{[1]} \mathbf{O}^{[2]} ... \mathbf{O}^{[M]} |R*\rangle, \end{aligned} \quad (9)$$

where the second line follows from the first by inserting the MPR Eq. (5). The observable matrices are given by

$$\mathbf{O}^{[i]} = \sum_{\tau_i} \sum_{\tau_i'} \langle \tau_i | \hat{O}^{[i]} | \tau_i' \rangle \mathbf{A}^{[i]\tau_i} \otimes \mathbf{A}^{\dagger[i]\tau_i'}, \quad (10)$$

$\langle L*| \equiv \langle L| \otimes \langle L|$ and $|R*\rangle \equiv |R\rangle \otimes |R\rangle$. The $\otimes$ is a tensor product[38]. From Eq. (10), calculation of the observable matrices has a computational cost of $O\left(Md^2\chi_e^4\right)$. Multiplication of these matrices according to Eq. (9) requires a further $O\left(M\chi_e^6\right)$ operations. Hence calculation of expectation values is efficient. I will discuss which operators correspond to important expectation values when I talk about the classical systems.

D. Errors in the TEBD algorithm

A useful property of the TEBD algorithm is that the size of its errors are known. The error resulting from the second order Suzuki-Trotter expansion is $O\left(\delta t^3\right)$. The size of this error is determined entirely by δt and so it is required that δt is small. Whether or not the value of δt used is too large can be identified by comparing a calculation to another using a small δt. If the differences are large then a smaller δt must be chosen. In practice it is the truncation of the MPR that produces the largest error. This is equal to the weight of the neglected Schmidt coefficients[30]. An indicator of the size of this error is the ratio of the largest and smallest untruncated Schmidt coefficients of a typical bipartite splitting, i.e. $\lambda_{\chi_k}^{[k]}/\lambda_1^{[k]}$. As truncation is performed at each time-step, this error accumulates with each time-step. So at large times t this error can become large. See [36] for a detailed analysis of the errors when studying spin chains.

III. STOCHASTIC LATTICE SYSTEMS

In this section, I introduce a class of stochastic classical 1D lattice systems that can be simulated by the TEBD algorithm. Their states are represented by a probability vector $|P(t)\rangle$, which is defined mathematically to be similar to $|\psi\rangle$, the state of the quantum systems in the previous section. It follows that $|P(t)\rangle$ can be described efficiently by an MPR in the same way as $|\psi\rangle$. I also show that $|P(t)\rangle$ evolves according to a Schrödinger-like equation. So the previous results for efficient time evolution of $|\psi\rangle$ apply to $|P(t)\rangle$. This abstract formulism is then made concrete by showing how it describes the TASEP.

A. The stochastic Schrödinger equation

The classical systems consist of M sites in a 1D lattice and each site may be in one of d configurations. Let each configuration of a site correspond to one of the d local basis states $|\tau\rangle$. The d^M possible configurations of the whole system correspond to the product states $|\boldsymbol{\tau}\rangle$, as defined for the quantum systems. The state of the classical system is represented by the probability vector

$$|P(t)\rangle = \sum_{\boldsymbol{\tau}} P(\boldsymbol{\tau}, t) |\boldsymbol{\tau}\rangle. \quad (11)$$

The coefficient $P(\boldsymbol{\tau}, t)$ is the probability that the system is in configuration $|\boldsymbol{\tau}\rangle$. This interpretation differs from the quantum case, where $|c_{\boldsymbol{\tau}}|^2$ is the probability of a particle being in state $|\boldsymbol{\tau}\rangle$ after measurement. In quantum mechanics Eq. (11) would correspond to the system being in a superposition of configurations. However, the classical system may only be in one configuration, the probability of which is given by the coefficients $P(\boldsymbol{\tau}, t)$. Equivalently, in the language of quantum mechanics, the classical state is a mixed state, rather than a pure state[38]. It follows that the normalisation of $|P(t)\rangle$ is different from the quantum case. The classical normalisation is

$$\sum_{\boldsymbol{\tau}} \langle \boldsymbol{\tau} | P(t) \rangle = \sum_{\boldsymbol{\tau}} P(\boldsymbol{\tau}, t) = 1. \quad (12)$$

Additionally it is required that $|P(t)\rangle$ be non-negative, as its entries are probabilities.

The system evolves stochastically with the rate $w(\boldsymbol{\tau}\to\boldsymbol{\tau}')$ governing the transition from configuration $\boldsymbol{\tau}$ to $\boldsymbol{\tau}'$. The transitions are Poisson processes, i.e. in a time dt the probability of a transition from $\boldsymbol{\tau}$ to $\boldsymbol{\tau}'$ is $w(\boldsymbol{\tau}\to\boldsymbol{\tau}')\,dt$. So, overall the system evolves according to the master equation[8]

$$\frac{\partial P(\boldsymbol{\tau},t)}{\partial t} = \sum_{\boldsymbol{\tau}'\neq\boldsymbol{\tau}} \big(P(\boldsymbol{\tau}',t)\,w(\boldsymbol{\tau}'\to\boldsymbol{\tau}) - P(\boldsymbol{\tau},t)\,w(\boldsymbol{\tau}\to\boldsymbol{\tau}')\big). \tag{13}$$

The first term on the right-hand side of Eq. (13) gives the rate of transitions into configuration $\boldsymbol{\tau}$ while the second term gives the rate out of $\boldsymbol{\tau}$. The master equation Eq. (13) may be rewritten in the form of a Schrödinger equation[9, 11]

$$\frac{\partial}{\partial t}|P(t)\rangle = H\,|P(t)\rangle\,. \tag{14}$$

To show this, multiply Eq. (14) from the left by $\langle\boldsymbol{\tau}|$ and use the resolution of the identity to obtain

$$\frac{\partial P(\boldsymbol{\tau},t)}{\partial t} = \sum_{\boldsymbol{\tau}'\neq\boldsymbol{\tau}} \left(\langle\boldsymbol{\tau}|H|\boldsymbol{\tau}'\rangle\,P(\boldsymbol{\tau}',t)\right) + \langle\boldsymbol{\tau}|H|\boldsymbol{\tau}\rangle\,P(\boldsymbol{\tau},t)\,. \tag{15}$$

Comparing the coefficients of $P(\boldsymbol{\tau},t)$ in Eqs. (13) and (15) one can see that the master equation is equivalent to the Schrödinger equation provided H is defined by

$$\langle\boldsymbol{\tau}|H|\boldsymbol{\tau}'\rangle = w(\boldsymbol{\tau}'\to\boldsymbol{\tau}) \quad \text{for} \quad \boldsymbol{\tau}\neq\boldsymbol{\tau}', \tag{16a}$$

$$\langle\boldsymbol{\tau}|H|\boldsymbol{\tau}\rangle = -\sum_{\boldsymbol{\tau}'\neq\boldsymbol{\tau}} w(\boldsymbol{\tau}\to\boldsymbol{\tau}')\,. \tag{16b}$$

This "stochastic Hamiltonian" H is not hermitian as in the quantum case, but following directly from Eqs. (16) it must satisfy

$$\sum_{\boldsymbol{\tau}}\langle\boldsymbol{\tau}|H|\boldsymbol{\tau}'\rangle = 0, \tag{17}$$

i.e. the columns of H add up to zero. This property can be regarded as a requirement for the conservation of probability, as it is equivalent to the statement that the rates leaving a configuration are equal to the sum of the rates entering other configurations from that configuration. In Sec. IV A, I show that it ensures that the normalisation of the state Eq. (12) is conserved in time.

B. Construction of the Hamiltonian

I now show how the stochastic Hamiltonian for any model can be constructed using Eqs. (16), using the TASEP as an example[21]. In the TASEP each site may either be occupied by a particle or empty. Accordingly, $\tau_i = \{0,1\}$, where 0 corresponds to an empty site and 1 corresponds to an occupied site. The processes of the TASEP are described in Fig. 1. First consider the injection of particles into site 1. As this process depends only on the configuration of that site, the other sites can be ignored. The process of injection corresponds to the transition rate

$$w(0\to 1) = \alpha. \tag{18}$$

By Eq. (16a) the non-zero off-diagonal element of its Hamiltonian is

$$\langle 1|H_L|0\rangle = \alpha. \tag{19}$$

The diagonal elements are found explicitly from Eq. (16b) or simply by requiring the columns to add to zero. This gives the Hamiltonian for this process as

$$H_L = \begin{pmatrix} -\alpha & 0 \\ \alpha & 0 \end{pmatrix}_1, \tag{20}$$

in the basis $\{|0\rangle,|1\rangle\}$. The subscript 1 indicates that the matrix acts on site 1. The Hamiltonian for the ejection of particles from the last site is similarly obtained and is given by

$$H_R = \begin{pmatrix} 0 & \beta \\ 0 & -\beta \end{pmatrix}_M. \tag{21}$$

The hopping process between site i and $i+1$ involves two sites and is represented by a two-site nearest-neighbour Hamiltonian. The hopping rate is $w(1,0\to 0,1) = p$. This gives the non-zero off-diagonal element $\langle 0|\langle 1|H_H|1\rangle|0\rangle = p$. Thus the hopping process Hamiltonian in the basis $\{|0\rangle|0\rangle,|0\rangle|1\rangle,|1\rangle|0\rangle,|1\rangle|1\rangle\}$ is

$$H_{Hi} = \begin{pmatrix} 0 & 0 & 0 & 0 \\ 0 & 0 & p & 0 \\ 0 & 0 & -p & 0 \\ 0 & 0 & 0 & 0 \end{pmatrix}_{i,i+1}. \tag{22}$$

Added together, the total Hamiltonian for the TASEP is

$$H = H_L + H_R + \sum_{i=1}^{M-1} H_{Hi}. \tag{23}$$

The Hamiltonians for each process may be added in this way because adding Hamiltonians is equivalent to adding the transition rates of different processes. It is easily demonstratable that the addition of two matrices satisfying Eq. (17) also satisfies this condition. Hamiltonians for more complicated models can be constructed in the same way and those used in this report are given in Appendix B.

IV. ADAPTING THE TEBD

Due to the mathematical similarity of the quantum and classical systems, the TEBD algorithm can be directly applied to simulate the classical systems by replacing $|\psi\rangle$ with $|P(t)\rangle$ and $-iH$ with H. The TEBD code was adapted in this way prior to this project by S. R. Clark and D. Jaksch. They also provided code to calculate simple classical expectation values, to be described in Sec. IV B. During the project I extended this code to calculate more complicated expectation values and modified it to study effects such as self-organisation. I also found some differences between the application of the algorithm to classical and quantum systems and some results that must be rederived. They are discussed in this section. With these aside, the methods and results of Sec. II apply equally for the classical systems.

A. Classical time evolution

In Sec. II B, I observed that the Suzuki-Trotter expansion preserves the normalisation of a quantum state. I have rederived this for the classical case, for which the Hamiltonian is not hermitian and evolution is not unitary. Both the norm and non-negativity of a probability vector are conserved when operated on by a stochastic matrix (SM). An SM is a square matrix with non-negative entries and columns adding to unity.

Multiplying the conservation of probability Eq. (17) by $P(\boldsymbol{\tau}')$ and summing over $\boldsymbol{\tau}'$ gives

$$\sum_{\boldsymbol{\tau}} \langle \boldsymbol{\tau} | H | P(t) \rangle = 0. \tag{24}$$

Adding a multiple of this to the normalisation condition Eq. (12) gives

$$\sum_{\boldsymbol{\tau}} \langle \boldsymbol{\tau} | cH + \mathbb{1} | P(t) \rangle = 1, \tag{25}$$

where c is a constant. So $cH + \mathbb{1}$ has columns adding to unity, and is an SM if all elements are positive. Using a well known expansion, the evolution operator may be written as

$$\mathrm{e}^{H\delta t} = \lim_{n\to\infty} \left(\mathbb{1} + \frac{H\delta t}{n} \right)^n. \tag{26}$$

The bracketed term has positive entries in the limit $n \to \infty$, assuming finite entries (no instantaneous processes), and so is an SM. The multiplication of two SMs must also have the properties of an SM. Thus $\mathrm{e}^{H\delta t}$ is an SM. It also follows from this that the Suzuki-Trotter expansion replaces one SM by a product of many. Hence I have shown that normalisation (and additionally non-negativity) is conserved in the classical case as well as the quantum case, up to truncation effects.

B. Classical expectation values

The calculation of expectation values in the classical case is different from that in the quantum case and requires fewer computations. The expectation value of a general product operator in the classical case is

$$\begin{aligned} &\sum_{\boldsymbol{\tau}} \langle \boldsymbol{\tau} | \hat{O}^{[1]} \otimes \hat{O}^{[2]} \otimes \ldots \otimes \hat{O}^{[M]} | P(t) \rangle \\ &= \langle L | \mathbf{O}^{[1]} \mathbf{O}^{[2]} \ldots \mathbf{O}^{[M]} | R \rangle, \end{aligned} \tag{27}$$

where

$$\mathbf{O}^{[i]} = \sum_{\tau_i} \sum_{\tau_i'} \langle \tau_i | \hat{O}^{[i]} | \tau_i' \rangle \mathbf{A}^{[i]\tau_i}. \tag{28}$$

Comparing this with Eq. (10) and using the same logic as Sec. II C, the calculation of expectation values in the classical case is also efficient and fewer operations are required due to the lack of a tensor product in Eq. (28).

Appendix A discusses which operators are used to generate the physically useful expectation values, such as particle density and flux.

C. The classical Schmidt decomposition

In Sec. II A, an interpretation of the Schmidt coefficients and vectors of an SD of a quantum system, was given in terms of two subsystems and their entanglement entropy. However, I have not found a similar interpretation for the SD of a classical system. An SD on a classical system gives $|P(t)\rangle = \sum_{\gamma_k=1}^{\chi_k} \lambda_{\gamma_k}^{[k]} \left| \phi_{\gamma_k}^{[1\ldots k]} \right\rangle \left| \phi_{\gamma_k}^{[k+1\ldots M]} \right\rangle$. However, the Schmidt vectors in general have negative coefficients and so cannot be interpreted as marginal probability vectors of their respective subsystems. This contrasts with the quantum SD, where they are basis states of their respective subsystems. Also, the Schmidt coefficients do not have a simple interpretation in terms of correlations (entanglement). Quantum unitary operations on $|\psi\rangle$ preserve the orthonormality of the Schmidt vectors, while classical operations on $|P(t)\rangle$ by an SM do not. As a result, a measure of correlations in terms of the Schmidt coefficients Eq. (3) does not exist for classical states. It remains a problem for future work to find, if possible, an interpretation of the SD for classical systems. The absence of this does not effect the accuracy or efficiency of the algorithm, as the mathematical formulism behind it is independent of any interpretation.

V. NUMERICAL DEMONSTRATIONS

Having shown that in principle the TEBD can be used to simulate classical stochastic systems, I now demonstrate how successful this is in practice by applying it to traffic models. First I show that the TEBD can

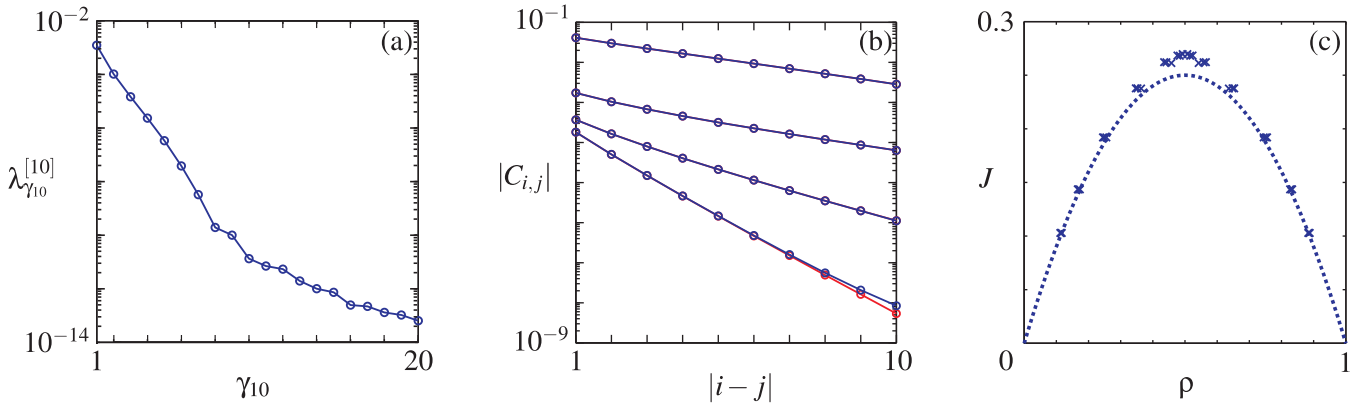

FIG. 2: The TASEP. (a) An example of the Schmidt coefficients $\lambda^{[10]}_{\gamma_{10}}$ for a splitting through the middle of the system. The decay is roughly exponential over 10 orders of magnitude, suggesting small truncation errors. Parameters used were $\alpha = 0.75$, $\beta = 0.5$. (b) Correlation functions in the TASEP decay exponentially, suggesting good approximation by a truncated MPR. Numerical results (blue) match analytical results (red) to about 10^{-6}. The (α,β) used, from top to bottom, were $(0.25,1.25)$, $(0.5,1)$, $(0.75,0.5)$ and $(1.25,1)$. (c) The fundamental diagram of the TASEP. See text for units. The dotted line corresponds to the analytical result in the limit that $M \to \infty$. Differences from the numerical results (crosses) are entirely due to the finite lattice size used, not inaccuracies in the algorithm. Steady-states took about 40 mins to calculate, with $M = 20$ and $\chi_e = 20$. A workstation with a 3GHz processor and 1GB of RAM was used for all calculations.

be used to calculate steady-states. The results are compared to exact analytical results for the TASEP and then more complicated models are solved, for which there are no analytical solutions. I then show that the TEBD can be used to simulate time evolution.

I derived operators to extract quantities, such as density and flux, from the simulations. These are discussed in Appendix A. All models, except for the TASEP, were constructed by me and details of their Hamiltonians are given in Appendix B.

A. Steady-state

1. *The TASEP*

Starting from a random configuration I evolved the TASEP in time, using the TEBD algorithm. The Schmidt coefficients' variations with time decreased as a steady-state was approached. When the variation decreased below a certain value the simulation ended and a steady-state was considered to be reached. As discussed in Sec. II A, the accuracy of the algorithm is dependent on the quick decay of the Schmidt coefficients. Fig. 2a shows their typical decay for the TASEP. The 10 orders of magnitude difference between the first and last Schmidt coefficient justifies the truncation to $\chi_e = 20$ and implies a negligible truncation error.

A natural feature of states represented by a truncated MPR is the exponential decay of the correlation function $C_{i,j} = \langle \tau_i \tau_j \rangle - \langle \tau_i \rangle \langle \tau_j \rangle$ with increasing $|i-j|$[24, 41]. This function represents the extent to which the densities at different sites are correlated. Using the analytical expressions derived in Appendix C, I have calculated correlation functions for a few typical α and β. Fig. 2b shows that the correlation functions do indeed decay exponentially. This suggests that these systems are well approximated by a truncated MPR. In Fig. 2b, I have also plotted the correlation functions calculated by the TEBD simulations. The agreement is excellent, with differences only becoming visible below 10^{-6}.

The TASEP can be interpreted in terms of traffic flow. It represents a simple model of a segment of a single carriageway, whose interaction with the rest of the road is through the injection and ejection rates of cars (particles) at the boundaries, α and β. Each lattice site is a point on the road which may or may not be occupied by a car. The distance between each site is $x \approx 5$m, which is the typical distance a car takes up on the road. The average speed of a car $v \approx 25\text{ms}^{-1}$ in an otherwise empty road is xp and thus $p = v/x \approx 5\text{s}^{-1}$. For my numerical calculations I set $p = 1$ and so transition rates, e.g. α and β, have units v/x and time has units x/v. I will write quantities as dimensionless, but their values in terms of typical distances and times can be found this way.

It is useful to know how the flux J (cars per unit time) through a road depends on the density ρ (cars per site). This is usually represented in a flux-density diagram, often referred to as the fundamental diagram (FD)[6], which is shown for the TASEP in Fig. 2c. Each cross corresponds to steady-state values of J and ρ, for a particular α and β, and the distribution of crosses gives the steady-state dependence of J on ρ. The TASEP FD captures the basic properties of the FDs of real roads: for

small ρ cars do not interact with each other and so their speeds do not depend on ρ, hence J is proportional to ρ. As ρ increases, interactions decrease the speeds of cars, and J reaches a maximum. It then reduces to zero as the road becomes increasingly jammed. The values of J and ρ calculated by the TEBD algorithm matched analytical results very well, with relative errors less than 10^{-6} and 10^{-5} respectively. Using the conversions of the previous paragraph J and ρ have the units cars v/x and cars$/x$ respectively.

2. *Two lanes*

Next the TEBD algorithm was used to find the steady-states of an extension of the TASEP to two lanes. Figs. 3a and 3b show the processes that take place in this model. Lane one and lane two have different injection rates (α_1 and α_2), ejection rates (β_1 and β_2) and hopping rates (p_1 and p_2), usually with lane one as the slow lane. Standard lane changing occurs from lane one to the corresponding site in lane two with rate c_1 and in the opposite direction with rate c_2. Another, more intelligent lane changing process gives particles additional rates I_1 and I_2 to change lane if the downstream neighbouring site is occupied but the other lane is empty, i.e. a particle will only change lanes if there is an advantage to being in the other lane. The implementation of this model with the formalism of Sec. III is described in Appendix B 1, including the transition rates and Hamiltonians for each process. The interpretation of this model in terms of traffic is similar to that for the TASEP, but generalised to two lanes. p_2 is set to unity for calculations, so x/v, v/x, cars v/x and cars$/x$ become the respective units for time, rates, J and ρ, where v is now the average speed in lane two if there were no other cars.

I investigated how lane changing effects the flux passing through a road. Fig. 3c shows the FD diagram for the two lane model, with and without lane changing. I found that lane changing increases the flux for a given density beyond that of two non-interacting lanes. This agrees with everyday experience at low densities, but not for high densities where the model fails to take into account the disruption of lane changing manoeuvres[42].

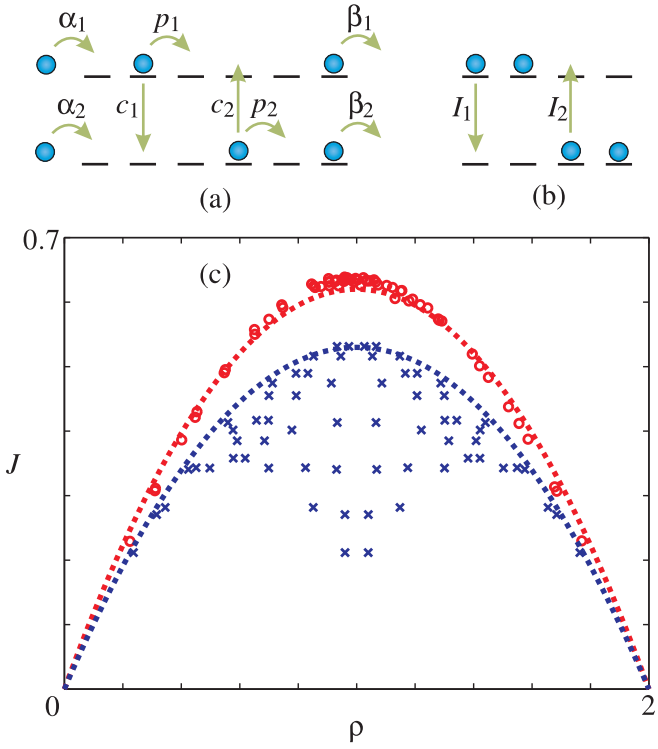

FIG. 3: The two lane model. (a) The processes and rates of the model with standard lane changing (refer to text). (b) Additional intelligent lane changing processes. (c) The FD diagram. See text for units. The figure shows that for the same density, the model with lane changing (red circles) has a greater flux than the model without (blue crosses). J and ρ now correspond to the combined flux and density in both lanes. The dotted lines are drawn to guide the eyes. $M = 20$, $p_1 = 0.7$ and $p_2 = 1$ were used along with a range of injection and ejection rates between 0 and 2. Lane changing rates, when non-zero, were $c_1 = c_2 = 0.2$, $I_1 = 0.8$ and $I_2 = 0$. Calculations took roughly 10 hours.

3. *Two species*

I also extended the TASEP to two species of particles, one of which may overtake the other. The model's processes are shown in Fig. 4a. Each species $i = 1, 2$ has its own injection, ejection and hopping rates α_i, β_i and p_i. Additionally a particle of species 1 may also swap with (overtake) a particle of species 2 with a rate p_3, if they are in neighbouring sites. Species 2 may not overtake species 1. The formalism behind this model is given in Appendix B 2. This can be interpreted as a simple model of lorries and cars on a single carriageway where lorries move slower than cars and cars may overtake lorries[43]. For calculations, p_1 was set to 1, making the units of time, rates, flux of cars J_c and density of cars ρ_c equal to x/v, v/x, cars v/x and cars$/x$ respectively, where v is the average speed of cars on an otherwise empty road.

I studied the effect of lorries on the FD of cars. The flux-density relationship for cars is shown in Fig. 4b for different lorry speeds p_2. The lorries have the effect of reducing the flux of cars for all car densities as well as shifting the peak of the curve to a lower density. The effect becomes extremely large for low lorry speeds, despite overtaking rates increasing as the lorries are slowed. This occurs because the density of lorries

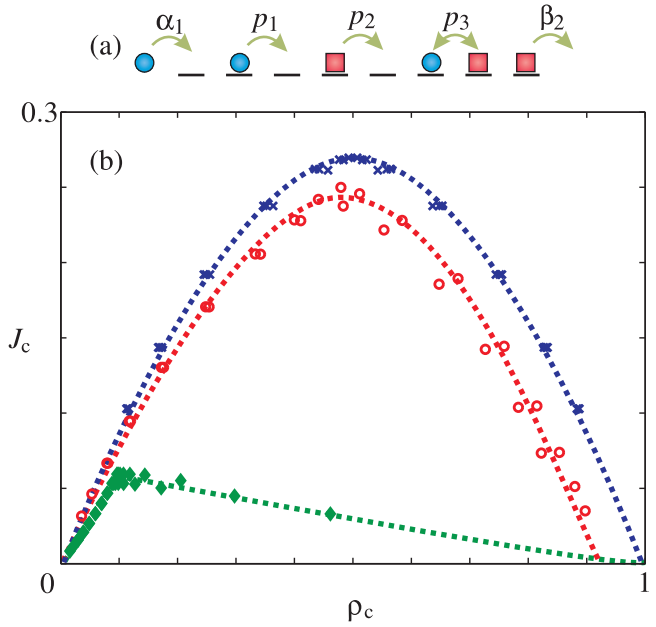

FIG. 4: The two species TASEP. (a) The processes and rates of this model. Although not shown here the rates α_2 and β_1 are included (refer to text). (b) The FD for cars, in the presence of lorries. See text for units. Flux-density values for cars are plotted for lorry speeds $p_2 = 1$ (red circles) and $p_2 = 0.1$ (green diamonds). Boundary parameters used were $\alpha_2 = 0.1$, $p_1 = 1$ and $\beta_2 = 2$. Overtaking was set as $p_3 = (p_1 - p_2)/3$. These flux-density values are compared with the absence of lorries (blue crosses) when $\alpha_2 = 0$, which is equivalent to the TASEP. The dotted lines are drawn to guide the eyes. Steady-states were calculated in $\approx$ 5h for $M = 20$ and $\chi_e = 20$.

increases as their speed is reduced (for fixed injection ratio). This causes cars to slow down, because their hopping is hindered. For the same reason, jamming occurs at lower car densities and the FD is compressed towards low densities. Promisingly, the shape of the FD with the presence of another species is much more similar to that of real roads[6], suggesting that only a few species of vehicle may be needed to produce realistic flux-density relationships.

B. Time evolution

Finally, I demonstrated that the TEBD algorithm could simulate the time evolution of a classical system. I did this for a model in which two independent lanes merge into a single lane, shown in Fig. 5a. Hopping from lanes one and two into the single lane is governed by the time dependent rates $l_1(t)$ and $l_2(t)$ respectively. Injection into lane one and two occurs at rates α_1 and α_2, and ejection out of the single lane occurs at a rate β. Lane changing does not occur before the merge, and for simplicity the hopping rate p is the same for all lattice sites. The Hamiltonian for this model is given in Appendix B 3.

I investigated how the TEBD algorithm could be used to optimise the settings of traffic lights. With the usual interpretation and units, I set $p = 1$. The traffic lights control the merge from two lanes to one, with a cycle period t_{cyc}. The cycles consist of alternate periods of $l_1 = 1$, $l_2 = 0$ (green for lane one) for a time t_1 and $l_1 = 0$, $l_2 = 1$ (green for lane two) for a time t_2. Between each of these periods is a dead-time where both rates are zero (red for both) for a time t_3. For fixed asymmetric injection rates α_1 and α_2, and ejection rate β, the cycle period t_{cyc} and dead-time t_3 were set, leaving the ratio t_2/t_1 as the only variable. I simulated the time evolution of the model over several cycles for a range of t_2/t_1. The average outgoing flux over a cycle J_{cyc} for each ratio was evaluated, and the ratio that maximises this was found. This is shown in Fig. 5b. The difference between a well and a badly optimised ratio is shown in Figs. 5c and 5d. From these figures it can be seen that the traffic light settings that optimise flux are those which keep the flux in each time period roughly the same. The optimising ratio of light times $t_2/t_1 = 0.27$ is larger than the ratios of the injection rates $\alpha_2/\alpha_1 = 0.1$. This seems to be a general feature of the model. An analytical approach to this kind of situation is given in [7].

C. Accuracy

The errors of the TEBD calculations can be easily determined. For the TASEP, two lane, two species and traffic light models the values of χ_e used were 20, 30, 20 and 50 respectively. The non-truncated Schmidt coefficients for a typical splitting decayed by 10, 7, 6 and 7 orders of magnitude respectively. Additionally, over the whole time period that the traffic light model was run, the total weight of the discarded Schmidt coefficients was typically of the order of 10^{-4}. So errors due to truncation were minimal, if not negligible; the systems could be accurately described by a low χ_e. Calculations used a time-step $\delta t = 10^{-2}$. I tested the magnitude of the error resulting from the Suzuki-Trotter expansion Eq. (8) for each model by repeating calculations with smaller δt. The differences between the two calculations for all models were negligible. This implies that $\delta t = 10^{-2}$ is small enough for a good approximation.

Several other models were investigated, but are not included here. It was found that the TEBD algorithm could also accurately simulate the steady-state or time evolution of these models, for reasonably low χ_e. This substantiates the main claim of this report: that the TEBD algorithm is able to efficiently simulate a range of classical systems. These other models included two

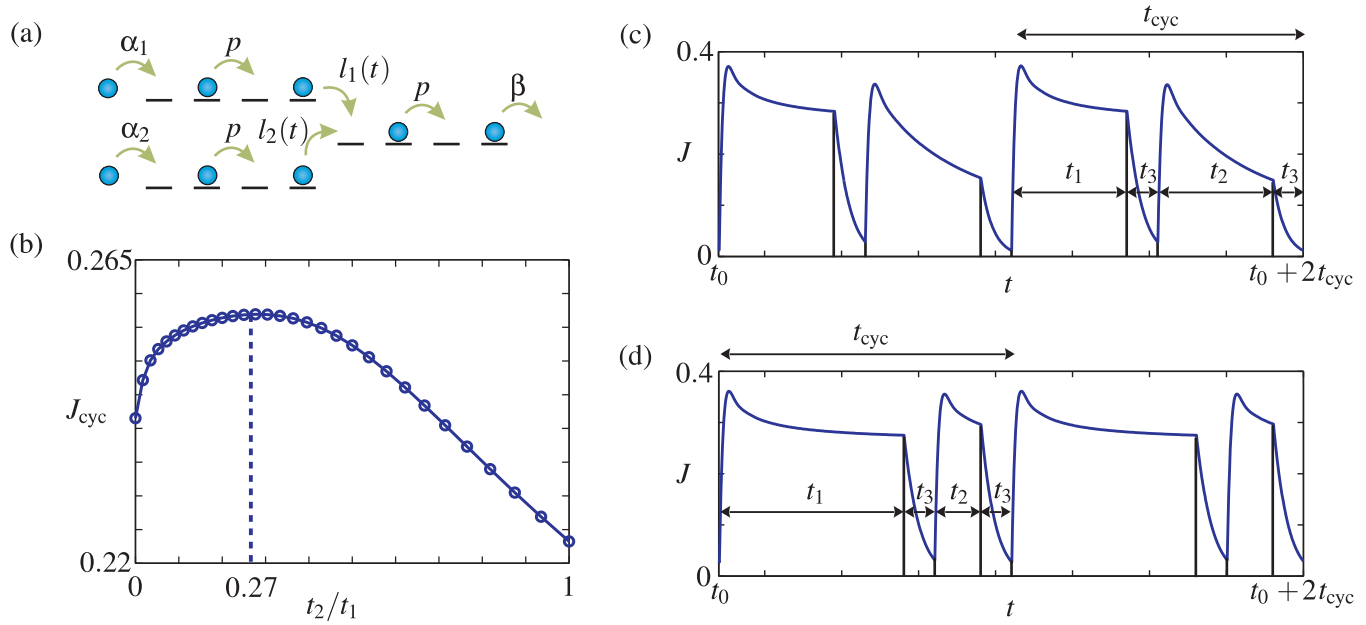

FIG. 5: The traffic light model. (a) Rates and processes (refer to text). (b) The average flux out of the system over a cycle J_{cyc}, calculated for several simulations with a range of ratios t_2/t_1. The maximising ratio is found to be 0.27. Rates were fixed as $\alpha_1 = 1$, $\alpha_2 = 0.1$ and $\beta = 1$, with $t_3 = 4$ and $t_{\text{cyc}} = 38$ (corresponding to about 30 seconds for typical urban traffic speeds). See text for units. (c) A badly optimised ratio $t_1/t_2 = 1$, where the flux in the period t_2 is noticeably smaller and thus less efficient. (d) A well optimised ratio $t_1/t_2 = 0.3$, where the flux in both t_1 and t_2 time periods are approximately even. A typical simulation over eight traffic light cycles took about 15 hours.

lanes with on and off ramps, temporary blockages of the TASEP and self-organisation by matching the boundary rates and densities at each time-step.

VI. CONCLUSIONS AND FURTHER WORK

I have applied the TEBD algorithm to successfully simulate classical systems, including time evolution away from steady-state. In particular, I have demonstrated that simple traffic models can be simulated efficiently and accurately, with small computation times, and investigated some simple applications of these models. This means that the TEBD algorithm is a promising candidate for studying the dynamics of a wide range of classical systems: vehicular traffic[6, 7, 15], biological transport[16–19], queuing[44] and communication networks[45]. It surpasses previous methods which are applicable to steady-states only.

The models used in this report were limited, for example only one-site and two-site nearest-neighbour Hamiltonians have been considered. Lifting this restriction to short range interactions would enable more complicated phenomena to be described, such as cars that accelerate or decelerate depending on the configuration of the road a few sites ahead of them. The required long distance interactions may be performed using two-site nearest-neighbour operations, by bringing lattice sites together using swap gates (operations that swap the configuration of two sites). The effect of the non-local interactions would be to increase the non-local correlations. As a result it is likely a greater χ_e and computation time would be needed for accurate simulation. However, this would make the models more physical and possibly lead to more realistic results. Another limitation was the restriction of 1D finite lattices. Since the TEBD algorithm was initially proposed in 2003 it has been extended and successfully applied to other geometries: tree-like structures[46], translationally invariant infinite 1D lattices[47], and infinite tree-like structures[48]. The tree-like structure naturally suits many systems, including traffic, queuing and communication networks, and so I propose that these extensions also be adapted to simulate such classical systems.

Acknowledgments

I would like to give huge thanks to both Stephen Clark and my supervisor Dieter Jaksch. They taught me a great deal about this topic and research in general. I apologise that I was not able to devise a way for them to shorten their commute to work.

[1] D.L. Schrank and T.J. Lomax, *The 2007 Urban Mobility Report (130001-09112007-PR)*, The Texas Transportation Institute (2007).

[2] K. Nagel, J. Esser and M. Rickert, *Large-Scale Traffic Simulations for Transport Planning*, Annu. Rev. Comp. Phys. (World Scientific, Singapore, 1992).

[3] M. J. Lighthill and G. B. Whitham, *On Kinematic Waves: II a Theory of Traffic Flow on Long Crowded Roads*, Proc. Roy. Soc. Lond. A **229**, 317 (1955).

[4] I. Prigogine and R. Herman, *Kinetic Theory of Vehicular Traffic* (American Elsevier Publishing Company, New York, 1971).

[5] K. Nagel and M. Schreckenberg, *A Cellular Automaton Model for Freeway Traffic*, J. Phys. I **2**, 2221 (1992).

[6] D. Chowdhury, L. Santen and A. Schadschneider, *Statistical Physics of Vehicular Traffic and Some Related Systems*, Phys. Rep. **329**, 199 (2000).

[7] D. Helbing, *Traffic and Related Self-Driven Many-Particle Systems*, Rev. Mod. Phys. **73**, 1067 (2001).

[8] R. A. Blythe and M. R. Evans, *Nonequilibrium Steady States of Matrix-Product Form: a Solver's Guide*, J. Phys. A **40**, R333 (2007).

[9] R. Stinchcombe, *Stochastic Non-Equilibrium Systems*, Adv. Phys. **50**, 431 (2001).

[10] B. Derrida, *An Exactly Soluble Non-Equilibrium System: The Asymmetric Exclusion Process*, Phys. Rep. **301**, 65 (1998).

[11] N. Rajewsky, L. Santen, A. Schadschneider and M. Schreckenberg, *The Asymmetric Exclusion Process: Comparison of Update Procedures*, J. Stat. Phys. **92**, 151 (2004).

[12] T. E. Harris, *Diffusion With 'Collisions' Between Particles*, J. Appl. Probab. **2**, 323 (1965).

[13] F. Spitzer, *Interaction of Markov Processes*, Adv. Math. **5**, 246 (1970).

[14] S. Sachdev, *Quantum Phase Transitions* (Cambridge University Press, Cambridge, 2001).

[15] A. Schadschneider, *Traffic Flow: a Statistical Physics Point of View*, Physica A **313**, 153 (2002).

[16] D. Chowdhury, A. Schadschneider and K. Nishinari, *Physics of Transport and Traffic Phenomena in Biology: From Molecular Motors and Cells to Organisms*, Phys. Life Rev. **2**, 318 (2005).

[17] Y. Aghababaie, G. I. Menon and M. Pilschke, *Universal Properties of Interacting Brownian Motors*, Phys. Rev. E **59**, 2578 (1999).

[18] T. Chou and D. Lohse, *Entropy-Driven Pumping in Zeolites and Biological Channels*, Phys. Rev. Lett. **82**, 3552 (1999).

[19] A. Parmeggiani, T. Franosch and E. Frey, *Phase Coexistence in Driven One-Dimensional Transport*, Phys. Rev. Lett. **90**, 086601 (2003).

[20] D. P. Landau and K. Binder, *A Guide to Monte Carlo Simulations in Statistical Physics (2nd edition)* (Cambridge University Press, Cambridge, 2005).

[21] B. Derrida, M. R. Evans, V. Hakim and V. Pasquier, *Exact Solution of a 1D Asymmetric Exclusion Model Using a Matrix Formulation*, J. Phys. A **26**, 1493 (2004).

[22] S. R. White, *Density Matrix Formulation for Quantum Renormalization Groups*, Phys. Rev. Lett. **69**, 2863 (1992).

[23] S. R. White, *Density-Matrix Algorithms for Quantum Renormalization Groups*, Phys. Rev. B **48**, 10345 (1993).

[24] U. Schollwöck, *The Density-Matrix Renormalisation Group*, Rev. Mod. Phys. **77**, 259 (2005).

[25] Y. Hieida, *Application of the Density Matrix Renormalization Group Method to a Non-Equilibrium Problem*, J. Phys. Soc. Jpn. **67**, 369 (1998).

[26] E. Carlon, M. Henkel and U. Schollwöck, *Density Matrix Renormalization Group and Reaction-Diffusion Processes*, Eur. Phys. J. B **12**, 99 (1999).

[27] E. Carlon, M. Henkel and U. Schollwöck, *Critical Properties of the Reaction-Diffusion Model* $2A \to 3A$, $2A \to 0$, Phys. Rev. E **63**, 036101 (2001).

[28] V. Popkov, M. Salerno and G. M. Schütz, *Asymmetric Simple Exclusion Process With Periodic Boundary Driving*, Phys. Rev. E **78**, 011122 (2008).

[29] G. Vidal, *Efficient Classical Simulation of Slightly Entangled Quantum Computations*, Phys. Rev. Lett. **91**, 147902 (2003).

[30] G. Vidal, *Efficient Simulation of One-Dimensional Quantum Many-Body Systems*, Phys. Rev. Lett. **93**, 040502 (2004).

[31] M. Fannes, B. Nachtergaele, and R. F. Werner, *Finitely Correlated States on Quantum Spin Chains*, Commun. Math. Phys. **144**, 443 (1992).

[32] D. Perez-Garcia, F. Verstraete, M. M. Wolf and J. I. Cirac, *Matrix Product State Representations*, Quant. Inf. Comput. **7**, 401 (2007).

[33] L. Amico, R. Fazio, A. Osterloh and V. Vedral, *Entanglement in Many-Body Systems*, Rev. Mod. Phys. **80**, 518 (2008).

[34] A. Perales and G. Vidal, *Entanglement Growth and Simulation Efficiency in One-Dimensional Quantum Lattice Systems*, Phys. Rev. A **78**, 042337 (2003).

[35] V. E. Korepin, *Universality of Entropy Scaling in One Dimensional Gapless Models*, Phys. Rev. Lett. **92**, 096402 (2004).

[36] D. Gobert, C. Kollath, U. Schollwöck and G. Schütz, *Real-Time Dynamics in Spin-1/2 Chains with Adaptive Time-Dependent Density Matrix Renormalization Group*, Phys. Rev. E **71**, 036102 (2005).

[37] S. R. Clark and D. Jaksch, *Efficient Dynamical Simulation of Strongly Correlated One-Dimensional Quantum Systems*, Lecture Notes in Computer Science 3743, 555 (2006).

[38] M. A. Nielson and I. L. Chuang, *Quantum Computation and Quantum Information* (Cambridge University Press, Cambridge, 2000).

[39] A J Daley, C Kollath, U Schollwck and G Vidal, *Time-Dependent Density-Matrix Renormalization-Group Using Adaptive Effective Hilbert Spaces*, J. Stat. Mech. P04005 (2004).

[40] M. Suzuki, *Fractal Decomposition of Exponential Operators with Applications to Many-Body Theories and Monte Carlo Simulations*, Phys. Lett. A **146**, 319 (1990); *General Theory of Fractal Path Integrals with Applications to Many-Body Theories and Statistical Physics*, J. Math. Phys. **32**, 400 (1991).

[41] S. Rommer and S. Östlund, *Class of Ansatz Wave Functions for One-Dimensional Spin Systems and Their Relation to the Density Matrix Renormalization Group*, Phys. Rev. B **55**, 2164 (1996).

[42] J. A. Laval and C. F. Daganzo, *Lane-Changing in Trac Streams*, Transport Research B **40**, 251 (2006).

[43] H. W. Lee, V. Popkov and D. Kim, *Two-Way Traffic Flow: Exactly Solvable Model of Traffic Jam*, J. Phys. A **30**, 8497 (1997).

[44] C. Furtlehner and J. Lasgouttes, *A Queueing Theory Approach For a Multi-Speed Exclusion Process*, Traffic and Granular Flow 07 (2007).

[45] A. Arenas, A. Diaz-Guilera and R. Guimera, *Communication in Networks with Hierarchical Branching*, Phys. Rev. Lett. **86**, 3169 (2001).

[46] Y. Y. Shi, L. M. Duan and G. Vidal, *Classical Simulation of Quantum Many-Body Systems With a Tree Tensor Network*, Phys. Rev. A **74**, 022320 (2006).

[47] G. Vidal, *Classical Simulation of Infinite-Size Quantum Lattice Systems in One Spatial Dimension*, Phys. Rev. Lett. **98**, 070201 (2007).

[48] D. Nagaj, E. Farhi, J. Goldstone, P. Shor and I. Sylvester, *Quantum Transverse-Field Ising Model on an Infinite Tree From Matrix Products States*, Phys. Rev. B **77**, 214431 (2008).

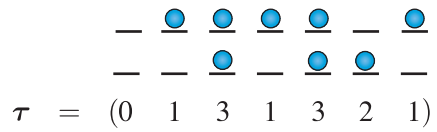

FIG. 6: Four possible configurations for each site are required for the two-lane model, corresponding to a site that is empty, has lane one occupied, has lane two occupied or has both lanes occupied.

Transitions	Rates
$\|0\rangle \to \|1\rangle$	α_1
$\|2\rangle \to \|3\rangle$	α_1
$\|0\rangle \to \|2\rangle$	α_2
$\|1\rangle \to \|3\rangle$	α_2

(a) Particle injection

Transitions	Rates
$\|1\rangle \to \|0\rangle$	β_1
$\|3\rangle \to \|2\rangle$	β_1
$\|2\rangle \to \|0\rangle$	β_2
$\|3\rangle \to \|1\rangle$	β_2

(b) Particle ejection

Transitions	Rates
$\|1\rangle \to \|2\rangle$	c_1
$\|2\rangle \to \|1\rangle$	c_2

(c) Unintelligent lane changing

Transitions	Rates
$\|1\rangle\|1\rangle \to \|2\rangle\|1\rangle$	I_1
$\|2\rangle\|2\rangle \to \|1\rangle\|2\rangle$	I_2

(d) Intelligent lane changing

Transitions	Rates
$\|1\rangle\|0\rangle \to \|0\rangle\|1\rangle$	p_1
$\|1\rangle\|2\rangle \to \|0\rangle\|3\rangle$	p_1
$\|3\rangle\|0\rangle \to \|2\rangle\|1\rangle$	p_1
$\|3\rangle\|2\rangle \to \|2\rangle\|3\rangle$	p_1
$\|2\rangle\|0\rangle \to \|0\rangle\|2\rangle$	p_2
$\|2\rangle\|1\rangle \to \|0\rangle\|3\rangle$	p_2
$\|3\rangle\|0\rangle \to \|1\rangle\|2\rangle$	p_2
$\|3\rangle\|1\rangle \to \|1\rangle\|3\rangle$	p_2

(e) Hopping

TABLE I: Transition rates for the two lane model.

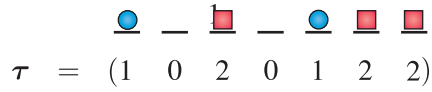

FIG. 7: In the two-species model there are only three possible configurations for each site: empty, occupied by species 1 or occupied by species 2.

Transitions	Rates
$\|0\rangle \to \|1\rangle$	α_1
$\|0\rangle \to \|2\rangle$	α_2

(a) Particle injection

Transitions	Rates
$\|1\rangle \to \|0\rangle$	β_1
$\|2\rangle \to \|0\rangle$	β_2

(b) Particle ejection

Transitions	Rates
$\|1\rangle\|0\rangle \to \|0\rangle\|1\rangle$	p_1
$\|2\rangle\|0\rangle \to \|0\rangle\|2\rangle$	p_2
$\|1\rangle\|2\rangle \to \|2\rangle\|1\rangle$	p_3

(c) Hopping

TABLE II: Transition rates for the two species model.

Transitions	Rates
$\|1\rangle\|0\rangle \to \|0\rangle\|1\rangle$	$l_1(t)$
$\|3\rangle\|0\rangle \to \|2\rangle\|1\rangle$	$l_1(t)$
$\|2\rangle\|0\rangle \to \|0\rangle\|1\rangle$	$l_2(t)$
$\|3\rangle\|0\rangle \to \|1\rangle\|1\rangle$	$l_2(t)$

TABLE III: The transitions and rates for the traffic light merge site.

Appendix A: Expectation values

Sec. IV B outlined how general expectation values could be calculated from some operators $\hat{O}^{[1]} \otimes \hat{O}^{[2]} \otimes ... \otimes \hat{O}^{[M]}$. Here I discuss which operators correspond to physical quantities, such as density and flux. I will not provide all of the generating operators used for the models in this report, but they are simple extensions of the ones presented here.

As an example I will give the operators corresponding to density and flux in the TASEP. In this model $|0\rangle$ and $|1\rangle$ correspond to an empty and occupied site respectively. The operator to extract the density at site i is simply

$$\hat{O}^{[i]} = \mathrm{diag}(0,1)_i, \tag{A1}$$

in the basis $\{|0\rangle, |1\rangle\}$. $\mathrm{diag}(a,b)$ simply means a diagonal matrix with diagonal entries a and b. By inserting this into the top line of Eq. (27), with all other operators the identity operator, one can show this is equal to

$P(\tau_i = 1, t) = \langle \tau_i \rangle$, as desired. The angled brackets imply that the expectation value is taken. For the flux at site i one wishes to calculate the probability that site i is occupied and site $i+1$ is empty. The operator to extract this is

$$\hat{O}^{[i]} \otimes \hat{O}^{[i+1]} = \mathrm{diag}(0,1)_i \otimes \mathrm{diag}(1,0)_{i+1}, \qquad \text{(A2)}$$

which inserted into the top line of Eq. (27) gives the expectation value $P(\tau_i = 1, \tau_{i+1} = 0, t) = \langle \tau_i (1 - \tau_{i+1}) \rangle$. The flux is this value multiplied by p. In a similar way, densities and fluxes of the more complicated models can be calculated from simple generating operators.

Appendix B: Hamiltonians

Here I present the Hamiltonians for the models focused on in the report: the two lanes, two species and traffic lights models.

1. Two lanes

I constructed the two lane extension to the TASEP by allowing each site to be in one of four possible configurations. I let $|\tau_i\rangle = \{|0\rangle, |1\rangle, |2\rangle, |3\rangle\}$ correspond to a site that is empty, occupied only in lane one, occupied only in lane two and occupied in both lanes. This is shown in Fig. 6. All figures and tables in this Appendix have been placed on page 13 for ease of reading the text.

The processes for this model are described in Section V A 2 and shown in Figs. 3a and 3b. These processes correspond to rates between configurations given in Table I. As outlined in Section III B these rates maybe transformed into Hamiltonians, which I present here. Injection into the first site is represented by the Hamiltonian

$$H_L^{2Ln} = \begin{pmatrix} -(\alpha_1+\alpha_2) & 0 & 0 & 0 \\ \alpha_1 & -\alpha_2 & 0 & 0 \\ \alpha_2 & 0 & -\alpha_1 & 0 \\ 0 & \alpha_2 & \alpha_1 & 0 \end{pmatrix}_1, \qquad \text{(B1)}$$

and ejection from site M by

$$H_R^{2Ln} = \begin{pmatrix} 0 & \beta_1 & \beta_2 & 0 \\ 0 & -\beta_1 & 0 & \beta_2 \\ 0 & 0 & -\beta_2 & \beta_1 \\ 0 & 0 & 0 & -(\beta_1+\beta_2) \end{pmatrix}_M. \qquad \text{(B2)}$$

The unintelligent lane changing at site i is represented by

$$H_{Ci}^{2Ln} = \begin{pmatrix} 0 & 0 & 0 & 0 \\ 0 & -c_1 & c_2 & 0 \\ 0 & c_1 & -c_2 & 0 \\ 0 & 0 & 0 & 0 \end{pmatrix}_i, \qquad \text{(B3)}$$

and the Hamiltonian for the intelligent lane changing at site i, H_{Ii}^{2Ln}, is given by

$$\begin{pmatrix} 0&0&0&0&0&0&0&0&0&0&0&0&0&0&0&0 \\ 0&0&0&0&0&0&0&0&0&0&0&0&0&0&0&0 \\ 0&0&0&0&0&0&0&0&0&0&0&0&0&0&0&0 \\ 0&0&0&0&0&0&0&0&0&0&0&0&0&0&0&0 \\ 0&0&0&0&0&0&0&0&0&0&0&0&0&0&0&0 \\ 0&0&0&0&0&-I_1&0&0&0&0&0&0&0&0&0&0 \\ 0&0&0&0&0&0&0&0&0&0&I_2&0&0&0&0&0 \\ 0&0&0&0&0&0&0&0&0&0&0&0&0&0&0&0 \\ 0&0&0&0&0&0&0&0&0&0&0&0&0&0&0&0 \\ 0&0&0&0&0&I_1&0&0&0&0&0&0&0&0&0&0 \\ 0&0&0&0&0&0&0&0&0&0&-I_2&0&0&0&0&0 \\ 0&0&0&0&0&0&0&0&0&0&0&0&0&0&0&0 \\ 0&0&0&0&0&0&0&0&0&0&0&0&0&0&0&0 \\ 0&0&0&0&0&0&0&0&0&0&0&0&0&0&0&0 \\ 0&0&0&0&0&0&0&0&0&0&0&0&0&0&0&0 \\ 0&0&0&0&0&0&0&0&0&0&0&0&0&0&0&0 \end{pmatrix}_{i,i+1}. \qquad \text{(B4)}$$

The Hamiltonian responsible for hopping between site i and $i+1$ is

$$H_{Hi}^{2Ln} = \begin{pmatrix}
0&0&0&0&0&0&0&0&0&0&0&0&0&0&0&0\\
0&0&0&0&p_1&0&0&0&0&0&0&0&0&0&0&0\\
0&0&0&0&0&0&0&0&p_2&0&0&0&0&0&0&0\\
0&0&0&0&0&0&p_1&0&0&p_2&0&0&0&0&0&0\\
0&0&0&0&-p_1&0&0&0&0&0&0&0&0&0&0&0\\
0&0&0&0&0&0&0&0&0&0&0&0&0&0&0&0\\
0&0&0&0&0&0&-p_1&0&0&0&0&0&p_2&0&0&0\\
0&0&0&0&0&0&0&0&0&0&0&0&0&p_2&0&0\\
0&0&0&0&0&0&0&0&-p_2&0&0&0&0&0&0&0\\
0&0&0&0&0&0&0&0&0&-p_2&0&0&p_1&0&0&0\\
0&0&0&0&0&0&0&0&0&0&0&0&0&0&0&0\\
0&0&0&0&0&0&0&0&0&0&0&0&0&0&p_1&0\\
0&0&0&0&0&0&0&0&0&0&0&0&-(p_1+p_2)&0&0&0\\
0&0&0&0&0&0&0&0&0&0&0&0&0&-p_2&0&0\\
0&0&0&0&0&0&0&0&0&0&0&0&0&0&-p_1&0\\
0&0&0&0&0&0&0&0&0&0&0&0&0&0&0&0
\end{pmatrix}_{i,i+1} . \tag{B5}$$

It follows that the total Hamiltonian for the two lane model is

$$H^{2Ln} = H_L^{2Ln} + H_R^{2Ln} + \sum_i^M H_{Ci}^{2Ln} + \sum_i^{M-1} \left(H_{Ii}^{2Ln} + H_{Hi}^{2Ln}\right). \tag{B6}$$

2. Two species

The two species TASEP was constructed by allowing three possible configurations at each site, i.e. $|\tau_i\rangle = \{|0\rangle, |1\rangle, |2\rangle\}$. I let these correspond to a site that is empty, occupied by a particle of species 1 or occupied by a site of species 2. Note that a site may not be occupied by two particles. A possible configuration is shown in Fig. 7. The processes for this model are described in Section V A 3. The rates corresponding to these processes are shown in Table II.

From this the Hamiltonians describing each process are

$$H_L^{2Sp} = \begin{pmatrix} -(\alpha 1+\alpha_2) & 0 & 0 \\ \alpha_1 & 0 & 0 \\ \alpha_2 & 0 & 0 \end{pmatrix}_1 , \tag{B7}$$

for the injection of particles into the first site,

$$H_R^{2Sp} = \begin{pmatrix} 0 & \beta_1 & \beta_2 \\ 0 & -\beta_1 & 0 \\ 0 & 0 & -\beta_2 \end{pmatrix}_M , \tag{B8}$$

for the ejection of particles from site M and

$$H_{Hi}^{2Sp} = \begin{pmatrix}
0&0&0&0&0&0&0&0&0\\
0&0&0&p_1&0&0&0&0&0\\
0&0&0&0&0&0&p_2&0&0\\
0&0&0&-p_1&0&0&0&0&0\\
0&0&0&0&0&0&0&0&0\\
0&0&0&0&0&-p_3&0&0&0\\
0&0&0&0&0&0&-p_2&0&0\\
0&0&0&0&0&p_3&0&0&0\\
0&0&0&0&0&0&0&0&0
\end{pmatrix}_{i,i+1} , \tag{B9}$$

describes the hopping from site i, including overtaking. The total Hamiltonian is

$$H^{2Sp} = H_L^{2Sp} + H_R^{2Sp} + \sum_i^{M-1} H_{Hi}^{2Sp}. \tag{B10}$$

3. Traffic lights

Sec. II B described the traffic light model, and its processes are shown in Fig. 5. To describe this, the same configurations as the two lane model were used with the 1st lane in the right hand half of the two lane model corresponding to the single lane in the traffic light model. The Hamiltonians for injection into the system are just the same as for the two lane model. The hopping either side of the merge site is just the same as for the two lane model with $p_1 = p_2 = p$ and the lane changing rates are set to zero. The ejection is the same, with $\beta_1 = \beta$. The value of p_2 on the right hand side of the merge site and β_2 could be set to anything because cars will not be allowed to enter that lane after the merge site.

The difference between the traffic light model and the two lane model is that a new Hamiltonian term is

required to describe the processes at the merge site. Let the site k correspond to the last site of the two independent lanes and site $k+1$ correspond to the first site of the single lane. Table III shows the rates between the configurations of sites k and $k+1$ that correspond to the lane merge processes. Using Eqs. (16) this results in the Hamiltonian

$$H^{\text{Merge}} = \begin{pmatrix}
0&0&0&0 & 0 & 0&0&0 & 0 & 0&0&0 & 0 & 0&0&0 \\
0&0&0&0 & l_1(t) & 0&0&0 & l_2(t) & 0&0&0 & 0 & 0&0&0 \\
0&0&0&0 & 0 & 0&0&0 & 0 & 0&0&0 & 0 & 0&0&0 \\
0&0&0&0 & 0 & 0&0&0 & 0 & 0&0&0 & 0 & 0&0&0 \\
0&0&0&0 & -l_1(t) & 0&0&0 & 0 & 0&0&0 & 0 & 0&0&0 \\
0&0&0&0 & 0 & 0&0&0 & 0 & 0&0&0 & l_2(t) & 0&0&0 \\
0&0&0&0 & 0 & 0&0&0 & 0 & 0&0&0 & 0 & 0&0&0 \\
0&0&0&0 & 0 & 0&0&0 & 0 & 0&0&0 & 0 & 0&0&0 \\
0&0&0&0 & 0 & 0&0&0 & -l_2(t) & 0&0&0 & 0 & 0&0&0 \\
0&0&0&0 & 0 & 0&0&0 & 0 & 0&0&0 & l_1(t) & 0&0&0 \\
0&0&0&0 & 0 & 0&0&0 & 0 & 0&0&0 & 0 & 0&0&0 \\
0&0&0&0 & 0 & 0&0&0 & 0 & 0&0&0 & 0 & 0&0&0 \\
0&0&0&0 & 0 & 0&0&0 & 0 & 0&0&0 & -(l_1(t)+l_2(t)) & 0&0&0 \\
0&0&0&0 & 0 & 0&0&0 & 0 & 0&0&0 & 0 & 0&0&0 \\
0&0&0&0 & 0 & 0&0&0 & 0 & 0&0&0 & 0 & 0&0&0 \\
0&0&0&0 & 0 & 0&0&0 & 0 & 0&0&0 & 0 & 0&0&0
\end{pmatrix}_{k,k+1}. \tag{B11}$$

The Hamiltonian for the whole model is

$$H^{\text{Lights}} = H_L^{2Ln} + H_R^{2Ln} + H_{\text{Merge}} + \sum_{i,i\neq k}^{M-1} H_{Hi}^{2Ln}. \tag{B12}$$

Appendix C: Solving the TASEP using an MPR

I calculated the analytical results shown in Sec. V from expressions derived by Derrida *et al.* in [21]. The derivation uses the MPR of the TASEP, complementing the TEBD algorithm. Here I overview how the expressions were obtained. The matrix product ansatz for the stationary state of the TASEP is

$$P(\boldsymbol{\tau},t) = \frac{1}{Z_M}\langle L|\mathbf{A}^{\tau_1}\mathbf{A}^{\tau_2}...\mathbf{A}^{\tau_M}|R\rangle. \tag{C1}$$

The important simplification in this case, compared to Eq. (5), is that while the matrix $\mathbf{A}^{\tau_i}$ depends on the configuration of the ith site, it does not depend on i. In the TASEP τ_i can take only 0 or 1 and so one may write

$$\mathbf{A}^{\tau_i} = \tau_i\mathbf{D} + (1-\tau_i)\mathbf{E}. \tag{C2}$$

Thus $\mathbf{A}^{\tau_i} = \{\mathbf{D},\mathbf{E}\}$, with $\mathbf{D}$ corresponding to an occupied site and $\mathbf{E}$ to an empty site.

By substituting the ansatz for $|P(t)\rangle$, Eq. (C1), into the equation $H|P(t)\rangle = 0$, Derrida *et al.* showed that for the steady state the ansatz is satisfied provided the following quadratic algebra is satisfied:

$$\mathbf{DE} = \mathbf{D} + \mathbf{E}, \tag{C3a}$$

$$\mathbf{D}|R\rangle = \frac{1}{\beta}|R\rangle, \tag{C3b}$$

$$\langle L|\mathbf{E} = \frac{1}{\alpha}\langle L|. \tag{C3c}$$

Several possible representations of $\mathbf{D}$, $\mathbf{E}$, $|R\rangle$ and $\langle L|$ were found that satisfy Eqs. (C3). For general α and β these matrices and boundary vectors are infinite dimensional.

Knowing such a representation exists Derrida *et al.* calculated the densities and correlations using only the quadratic algebra of Eqs. (C3). Firstly, defining the useful matrix $\mathbf{C} = \mathbf{D} + \mathbf{E}$ the normalisation is given by $Z_M = \langle L|\mathbf{C}^M|R\rangle$ as expanding $\mathbf{C}^M = (\mathbf{D}+\mathbf{E})^M$ gives all of the possible configurations of the system. Using Eqs. (C3) and fixing the normalisation with $\langle L|R\rangle = 1$, they showed

$$\langle L|\mathbf{C}^M|R\rangle = \sum_{i=1}^{M} \frac{i(2M-1-i)!}{M!(M-i)!}\frac{(p/\beta)^{i+1}-(p/\alpha)^{i+1}}{p/\beta - p/\alpha}. \tag{C4}$$

The particle density at site i is just the sum of the probabilities of configurations with site i occupied,

$$\langle\tau_i\rangle_M = \frac{1}{Z_M}\langle L|\mathbf{C}^{i-1}\mathbf{D}\mathbf{C}^{M-i}|R\rangle, \tag{C5}$$

which again using only Eqs. (C3) reduces to

$$\langle \tau_i \rangle_M = \sum_{j=0}^{M-i-1} \frac{(2j)!}{j!(j+1)!} \frac{Z_{M-1-j}}{Z_M} + \frac{Z_{i-1}}{Z_M} \sum_{j=2}^{M-i+1} \frac{(j-1)(2M-2i-j)!}{(M-i)!(M-i-j+1)!} \left(\frac{p}{\beta}\right)^j, \quad \text{(C6)}$$

for $i < M$, and for the case $i = M$,

$$\langle \tau_M \rangle_M = \frac{p}{\beta} \frac{Z_{M-1}}{Z_M}. \quad \text{(C7)}$$

Similarly, two-point functions can be expressed in terms of the densities,

$$\langle \tau_i \tau_j \rangle_M = \sum_{k=0}^{M-j-1} \frac{(2k)!}{k!(k+1)!} \frac{Z_{M-k-1}}{Z_M} \langle \tau_i \rangle_{M-k-1} + \langle \tau_i \rangle_{j-1} \frac{Z_{j-1}}{Z_M} \sum_{k=2}^{M-j+1} \frac{(k-1)(2M-2j-k)!}{(M-j)!(M-j-k+1)!}, \quad \text{(C8)}$$

for $1 \le i < j \le M-1$. A special case is the particle flux

$$p\langle \tau_i (1-\tau_{i+1}) \rangle = \frac{1}{Z_M} \langle L | \mathbf{C}^{i-1} \mathbf{DEC}^{M-i-1} | R \rangle, \quad \text{(C9)}$$

$$= p \frac{Z_{M-1}}{Z_M}, \quad \text{(C10)}$$

where to get to the second line Eq. (C3a) has been used. From this we see that the flux doesn't depend on the site in the steady state, as one would expect due to the conservation of particles.